Nuclear Science and Techniques (2024) 35:95
https://doi.org/10.1007/s41365-024-01452-y

Possibilities for the synthesis of superheavy element $Z = 121$ in fusion reactions

Ming-Hao Zhang[1,2] · Yu-Hai Zhang[1,2] · Ying Zou[1,2] · Xiu-Xiu Yang[1,2] · Gen Zhang[3] · Feng-Shou Zhang[1,2,4]

Received: 14 December 2023 / Revised: 11 March 2024 / Accepted: 16 March 2024 / Published online: 18 June 2024

Abstract
Based on the dinuclear system model, the calculated evaporation residue cross sections matched well with the current experimental results. The synthesis of superheavy elements $Z = 121$ was systematically studied through combinations of stable projectiles with $Z = 21$–30 and targets with half-lives exceeding 50 d. The influence of mass asymmetry and isotopic dependence on the projectile and target nuclei was investigated in detail. The reactions ^{254}Es (^{46}Ti, 3n) ^{297}121 and ^{252}Es (^{46}Ti, 3n) ^{295}121 were found to be experimentally feasible for synthesizing superheavy element $Z = 121$, with maximal evaporation residue cross sections of 6.619 and 4.123 fb at 219.9 and 223.9 MeV, respectively.

Keywords Superheavy nuclei · Dinuclear system model · Fusion reaction · Evaporation residue cross section

1 Introduction

The production of new superheavy nuclei (SHN) is a challenging frontier in low-energy nuclear reactions. Over the years, experimental and theoretical nuclear physicists have explored SHN synthesis since the prediction of the "island of stability" around $Z = 114$, $N = 184$ [1, 2]. The Skyrme–Hartree–Fock method considers $Z = 120$, 124, or 126 and $N = 172$ or 184 as magic numbers [3]. The synthesis of superheavy elements (SHEs) $Z = 107$–112 was accomplished in GSI using cold fusion reactions with Pb and Bi targets [4]. However, despite the successful synthesis of SHE $Z = 113$ via the cold fusion reaction ^{70}Zn + ^{209}Bi at RIKEN [5], the evaporation residue cross section (ERCS) σ_{ER} was only 0.03 pb, reaching the limit of experimental detection at that time [6]. To overcome this challenge, researchers in Dubna focused on hot fusion reactions with ^{48}Ca beams and actinide targets. This method produces SHEs with $Z = 114$–118 [7–12], which complete the seventh period of the periodic table.

In recent years, several new isotopes with $Z \leq 118$ have been synthesized using modern accelerators, such as the DC-280 and U-400 of the Dubna SHE factory, RILAC of RIKEN, SFC of HIRFL, and UNILAC of GSI [7, 12–16]; however, the production of SHEs with $Z > 118$ remains a challenge. Previous attempts to produce SHEs with $Z = 120$ using ^{58}Fe+^{244}Pu [6] and ^{54}Cr + ^{248}Cm [17] reactions at Dubna and GSI, respectively, did not observe any α decay chains associated with this element. The three events reported by the GSI in Ref. [17] were later determined to be random events [18]. In 2020, with the gas-filled recoil separator TASCA at GSI, the search for synthesizing SHEs with $Z = 119$ and $Z = 120$ was conducted via the reactions ^{50}Ti + ^{249}Bk and ^{50}Ti + ^{249}Cf, yet neither was detected [19]. In 2022, RIKEN estimated the optimal incident energy for synthesizing SHE $Z = 119$ through the reaction ^{51}V+^{248}Cm [20]. Therefore, the synthesis of SHEs $Z > 118$ requires not only more advanced detection and identification techniques but also an appropriate reaction system.

This work was supported by the National Key R &D Program of China (No. 2023YFA1606401) and the National Natural Science Foundation of China (Nos. 12135004, 11635003 and 11961141004).

✉ Feng-Shou Zhang
fszhang@bnu.edu.cn

1 The Key Laboratory of Beam Technology of Ministry of Education, College of Nuclear Science and Technology, Beijing Normal University, Beijing 100875, China

2 Institute of Radiation Technology, Beijing Academy of Science and Technology, Beijing 100875, China

3 School of Physical Science and Technology, Guangxi University, Nanning 530004, China

4 National Laboratory of Heavy Ion Accelerator of Lanzhou, Center of Theoretical Nuclear Physics, Lanzhou 730000, China

Several models and different fusion mechanisms have been proposed to accurately describe the process of fusion-evaporation reactions. The improved quantum molecular dynamics (ImQMD) model [21], time-dependent Hartree-Fock theory [22–25], fusion-by-diffusion model [26], cluster dynamical decay model [27], two-step model [28, 29], dinuclear system (DNS) model [30–44], and other methods [45–48] have proved to be reliable in reproducing experimental data and have provided predictions about the synthesis of unknown nuclei [22, 45, 49–56].

The synthesis and decay of elements $Z = 119$ and $Z = 120$ have been extensively studied [22, 33, 35, 45, 52, 57–59], whereas only a limited number of calculations have been conducted for the synthesis of SHE $Z = 121$. To address this research gap, this study aims to investigate the optimal projectile-target combinations for synthesizing SHE $Z = 121$ and provide a reference for future experimental attempts.

The remainder of this paper is organized as follows: In Sect. 2, the DNS model is described, and its reliability is examined. The ERCSs of $Z = 121$ isotopes in different reaction channels are discussed in Sect. 3. Finally, the conclusions are provided in Sect. 4.

2 Theoretical descriptions

In the DNS model, the ERCS for synthesizing SHN in the center-of-mass frame can be obtained using the following expression:

$$\sigma_{\mathrm{ER}}(E_{\mathrm{c.m.}}) = \frac{\pi\hbar^2}{2\mu E_{\mathrm{c.m.}}} \sum_J (2J+1) T(E_{\mathrm{c.m.}}, J) \times P_{\mathrm{CN}}(E_{\mathrm{c.m.}}, J) W_{\mathrm{sur}}(E_{\mathrm{c.m.}}, J). \tag{1}$$

Here, $T\left(E_{\mathrm{c.m.}}, J\right)$ represents the transmission probability of the colliding system overcoming the Coulomb barrier V_{b}. $P_{\mathrm{CN}}\left(E_{\mathrm{c.m.}}, J\right)$ is the fusion probability for the formation of a compound nucleus [60]. $W_{\mathrm{sur}}\left(E_{\mathrm{c.m.}}, J\right)$ denotes the probability that the excited compound nucleus emits neutrons instead of undergoing fission to reach the ground state [61]. The nucleus–nucleus interaction potential considering quadrupole deformation is expressed as follows [62]:

$$V(R, \beta_1, \beta_2, \theta_1, \theta_2) = \frac{1}{2}C_1(\beta_1 - \beta_1^0)^2 + \frac{1}{2}C_2(\beta_2 - \beta_2^0)^2 + V_{\mathrm{C}}(R, \beta_1, \beta_2, \theta_1, \theta_2) + V_{\mathrm{N}}(R, \beta_1, \beta_2, \theta_1, \theta_2), \tag{2}$$

where $\beta_{1,2}$ and $\beta_{1,2}^0$ denote the dynamic quadrupole and static deformation parameters of the projectile and target nucleus, respectively. $\theta_{1,2}$ are the collision angles of the deformed projectile and target nucleus, respectively. The stiffness parameters $C_{1,2}$ are expressed as follows [63]:

$$C_i = (\lambda - 1)\left[(\lambda + 2)R_{0,i}^2\sigma - \frac{3}{2\pi}\frac{Z_i^2 e^2}{R_{0,i}(2\lambda + 1)}\right]. \tag{3}$$

$\lambda = 2$ represents the quadrupole deformation. The Coulomb potential V_{C} is determined using Wang's formula [64]:

$$V_{\mathrm{C}}(R, \beta_1, \beta_2, \theta_1, \theta_2) = \frac{Z_1 Z_2 e^2}{R} + \sqrt{\frac{9}{20\pi}}\frac{Z_1 Z_2 e^2}{R^3} \times \sum_{i=1,2} R_i^2 \beta_2^{(i)} P_2(\cos\theta_i) + \frac{3}{7\pi} \times \frac{Z_1 Z_2 e^2}{R^3} \sum_{i=1,2} R_i^2 [\beta_2^{(i)} P_2(\cos\theta_i)]^2. \tag{4}$$

The nuclear potential V_{N} is given by the Woods–Saxon potential [64]:

$$V_{\mathrm{N}}(R, \beta_1, \beta_2, \theta_1, \theta_2) = -V_0 \times \left\{1 + \exp\left[\frac{r - \sum_{i=1,2} R_i\left(1 + \sqrt{5/4\pi}\beta_2^{(i)} P_2(\cos\theta_i)\right)}{a}\right]\right\}^{-1}. \tag{5}$$

During the capture process, the transmission probability $T(E_{\mathrm{c.m.}}, B, J)$ is described using Ahmed's formula [65, 66]:

$$T(E_{\mathrm{c.m.}}, B, J) = \frac{1 - \exp(-4\pi\alpha)}{1 + \exp(2\pi(\beta_J - \alpha))}. \tag{6}$$

Here $\alpha = \frac{\sqrt{2\mu E_{\mathrm{c.m.}}}}{\hbar}\alpha_{\mathrm{M}}$ and $\beta_J = \frac{\sqrt{2\mu\left(B + \frac{\hbar^2}{2\mu R_{\mathrm{B}}^2(J)}J(J+1)\right)}}{\hbar}\alpha_{\mathrm{M}}$. μ represents the reduced mass, and α_{M} denotes the Morse parameter [67].

Considering the barrier distribution function $f(B)$, $T\left(E_{\mathrm{c.m.}}, J\right)$ can be written as:

$$T\left(E_{\mathrm{c.m.}}, J\right) = \int f(B) T\left(E_{\mathrm{c.m.}}, B, J\right) \mathrm{d}B. \tag{7}$$

The asymmetric barrier distribution parameters are presented in Refs. [68]. The capture cross section σ_{cap} is calculated as follows [62]:

$$\sigma_{\mathrm{cap}}\left(E_{\mathrm{c.m.}}\right) = \frac{\pi\hbar^2}{2\mu E_{\mathrm{c.m.}}} \sum_J (2J+1) T\left(E_{\mathrm{c.m.}}, J\right). \tag{8}$$

The fusion of the colliding nuclei is determined by the potential energy surface, expressed as [62]

$$U\left(N_1, Z_1, N_2, Z_2, R, \beta_1, \beta_2\right) = E_{\mathrm{B}}\left(N_1, Z_1\right) + E_{\mathrm{B}}\left(N_2, Z_2\right) - E_{\mathrm{B}}\left(N_3, Z_3\right) + V_{\mathrm{CN}}\left(N_1, Z_1, N_2, Z_2, R, \beta_1, \beta_2\right). \tag{9}$$

The data of the binding energies of the colliding nucleus $E_{\mathrm{B}}\left(N_{1,2}, Z_{1,2}\right)$ and the formed compound nucleus $E_{\mathrm{B}}\left(N_3, Z_3\right)$

is taken from Ref. [69]. V_{CN} denotes the nucleus–nucleus interaction potential.

Nucleon transfer is treated as a diffusion process at the lowest point on the potential energy surface, known as the driving potential [62]. To form a compound nucleus, the dinuclear system must surpass the inner fusion barrier B_{fus} along the mass asymmetry degree $\eta = (A_{\mathrm{P}} - A_{\mathrm{T}})/(A_{\mathrm{P}} + A_{\mathrm{T}})$, which denotes the potential energy disparity between the incident point and the Businaro–Gallone (B.G.) point (the peak of the driving potential) [70], defined as $B_{\mathrm{fus}} = U(\eta_{\mathrm{B.G.}}) - U(\eta_{\mathrm{i}})$. The fusion probability $P_{\mathrm{CN}}(E_{\mathrm{c.m.}}, J)$ is determined through the summation of the distribution probabilities of crossing the B.G. point $P(N_1, Z_1, E_1, t)$ as follows:

$$P_{\mathrm{CN}}(E_{\mathrm{c.m.}}, J) = \sum_{N_1=1}^{N_{\mathrm{B.G.}}} \sum_{Z_1=1}^{Z_{\mathrm{B.G.}}} P(N_1, Z_1, E_1, t = \tau_{\mathrm{int}}(J)). \tag{10}$$

Here, the interaction time $\tau_{\mathrm{int}}(J)$ is calculated using the deflection function method [71]. $P(N_1, Z_1, E_1, t)$ is calculated by solving the two-dimensional master equation.

$$\begin{aligned}
&\frac{\mathrm{d}P(N_1, Z_1, E_1, t)}{\mathrm{d}t} \\
&= \sum_{N_1'} W_{N_1,Z_1;N_1',Z_1}(t) \\
&\quad \times [d_{N_1,Z_1} P(N_1', Z_1, E_1, t) - d_{N_1',Z_1} P(N_1, Z_1, E_1, t)] \\
&+ \sum_{Z_1'} W_{N_1,Z_1;N_1,Z_1'}(t) \\
&\quad \times [d_{N_1,Z_1} P(N_1, Z_1', E_1, t) - d_{N_1,Z_1'} P(N_1, Z_1, E_1, t)] \\
&- [\Lambda_{\mathrm{qf}}(\Theta(t)) + \Lambda_{\mathrm{fis}}(\Theta(t))] P(N_1, Z_1, E_1, t).
\end{aligned} \tag{11}$$

Here $W_{N_1,Z_1;N_1',Z_1}$ denotes the mean transition probability from state (N_1, Z_1) to state (N_1', Z_1) [72], and d_{N_1,Z_1} is the microscopic dimension of state (N_1, Z_1). The quasi-fission rate Λ_{qf} and fission rate Λ_{fis} are given by the one-dimensional Kramers formula [73].

The survival process is determined primarily by the rivalry between fission and neutron emissions [74]. The survival probability at excitation energy E^*_{CN} can be expressed as

$$\begin{aligned}
&W_{\mathrm{sur}}(E^*_{\mathrm{CN}}, x, J) \\
&= P(E^*_{\mathrm{CN}}, x, J) \prod_{i=1}^{x} \left[\frac{\Gamma_{\mathrm{n}}(E_i^*, J)}{\Gamma_{\mathrm{n}}(E_i^*, J) + \Gamma_{\mathrm{f}}(E_i^*, J)} \right].
\end{aligned} \tag{12}$$

$P(E^*_{\mathrm{CN}}, x, J)$ denotes the realization probability of emitting x neutrons [75]. E_i^* represents the excitation energy of a compound nucleus that emits $i - 1$ neutrons [57].

The neutron decay width $\Gamma_{\mathrm{n}}(E_i^*, J)$ was calculated using the Weisskopf–Ewing theory [76]:

$$\begin{aligned}
\Gamma_{\mathrm{n}}(E_i^*, J) &= \frac{(2s_{\mathrm{n}} + 1) m_{\mathrm{n}}}{\pi^2 \hbar^2 \rho(E_i^*, J)} \\
&\quad \times \int_{I_{\mathrm{n}}} \varepsilon \rho(E_i^* - B_{\mathrm{n}} - \varepsilon, J) \sigma_{\mathrm{inv}}(\varepsilon) \mathrm{d}\varepsilon.
\end{aligned} \tag{13}$$

Here, $I_{\mathrm{n}} = \left[0, E_i^* - B_{\mathrm{n}} - \delta - \frac{1}{a}\right]$. δ and B_{n} represent the pairing correction and the neutron separation energies [33], respectively. The level density ρ is expressed as in Refs. [77], and σ_{inv} denotes the inverse reaction cross section [78].

$\Gamma_{\mathrm{f}}(E_i^*, J)$ is the fission decay width given by the Bohr–Wheeler transition-state method [79]:

$$\begin{aligned}
\Gamma_{\mathrm{f}}(E_i^*, J) &= \frac{1}{2\pi \rho_{\mathrm{f}}(E_i^*, J)} \\
&\quad \times \int_{I_{\mathrm{f}}} \frac{\rho_{\mathrm{f}}(E_i^* - B_{\mathrm{f}}(E_i^*, J) - \varepsilon, J) \mathrm{d}\varepsilon}{1 + \exp\left[-2\pi (E_i^* - B_{\mathrm{f}}(E_i^*, J) - \varepsilon)/\hbar\omega\right]},
\end{aligned} \tag{14}$$

with $I_{\mathrm{f}} = \left[0, E_i^* - B_{\mathrm{f}}(E_i^*, J) - \delta - \frac{1}{a_{\mathrm{f}}}\right]$, $a_{\mathrm{f}} = 1.1A/12$ [80, 81]. The temperature-dependent fission barrier $B_{\mathrm{f}}(E_i^*, J)$ was calculated using the following expression [82, 83]:

$$\begin{aligned}
B_{\mathrm{f}}(E_i^*, J) &= B_{\mathrm{f}}^{\mathrm{LD}}(1 - x_{\mathrm{LD}} T_i^2) \\
&\quad + B_{\mathrm{f}}^{\mathrm{M}}(E_i^* = 0, J) \exp\left(-\frac{E_i^*}{E_{\mathrm{D}}}\right) \\
&\quad - \left(\frac{\hbar^2}{2J_{\mathrm{g.s.}}} - \frac{\hbar^2}{2J_{\mathrm{s.d.}}}\right) J(J+1),
\end{aligned} \tag{15}$$

where $B_{\mathrm{f}}{}^{\mathrm{LD}}$ denotes the macroscopic portion of the fission barrier. T_i and x_{LD} represent the nuclear temperature and temperature-dependent parameters, respectively, [82]. $B_{\mathrm{f}}{}^{\mathrm{M}}$ is the microscopic shell correction energy in the ground state [69] and $E_{\mathrm{D}} = 25$ MeV [50]. $J_{\mathrm{g.s.}}$ and $J_{\mathrm{s.d.}}$ are as expressed in Refs. [84, 85].

To evaluate the accuracy of our model in predicting the ERCSs of SHN, Fig. 1 presents the comparisons between the calculated ERCSs and the experimental data in the reactions ^{48}Ca + ^{245}Cm [12, 86], ^{48}Ca + ^{248}Cm [87], ^{48}Ca + ^{249}Bk [88] and ^{48}Ca + ^{249}Cf [12, 89, 90]. Calculation uncertainties arise from the relatively subjective choice of the E_{D} range [91]. The fission barrier relies heavily on the contribution of the shell correction energy, and the reduction in the shell correction energy with increasing excitation energy is described by E_{D} values, which lie in the range of $10\ \mathrm{MeV} \le E_{\mathrm{D}} \le 30\ \mathrm{MeV}$ [92].

As shown in Fig. 1a–d, the ERCSs show a decreasing trend with increasing proton number of compound nucleus. For the reactions ^{48}Ca + ^{245}Cm and ^{48}Ca + ^{249}Cf, the maximal ERCSs of both the calculation and experiment appeared in the 3n-emission channels. The 4n-emission channels are more favorable for the synthesis of SHN with the reactions

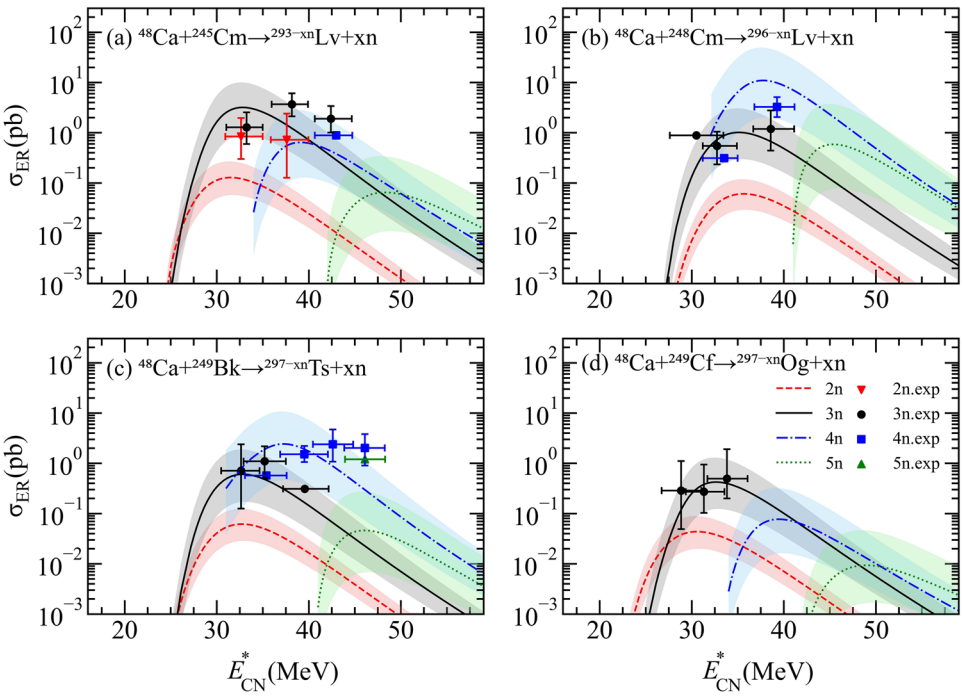

Fig. 1 (Color online) Comparison of the predicted ERCSs with the experimental results [12, 86–90] for the synthesis of Lv (**a**, **b**), Ts (**c**), and Og (**d**). The calculated ERCSs in the 2n-, 3n-, 4n-, and 5n-emission channels are denoted by the dashed, solid, dash-dot, and dotted lines, respectively. The shades indicate the uncertainties of the calculated ERCSs. The experimental results for the 2n-, 3n-, 4n-, and 5n-emission channels are denoted by inverted triangles, circles, squares and triangles, respectively

^{48}Ca + ^{248}Cm and ^{48}Ca + ^{249}Bk. The predicted ERCSs aligned well with the experimental results, particularly for the reaction ^{48}Ca + ^{249}Cf. A maximal ERCS of $0.42^{+0.87}_{-0.30}$ pb for the reaction ^{48}Ca + ^{249}Cf was predicted at the 3n-emission channel at E^*_{CN} = 32.0 MeV. This is consistent with the experimental value of $0.5^{+1.6}_{-0.3}$ pb with $E^*_{CN} = 32.1 - 36.6$ MeV in the same channel. This validates the applicability of the DNS model for predicting the synthesis of new elements via fusion–evaporation reactions.

3 Results and discussion

To prevent facility contamination by unstable beams, we chose stable projectiles with Z = 21–30 and actinide targets with half-lives exceeding 50 d for the experimental duration; the optimal reaction systems are summarized in Table 1. The most favorable reactions and ERCSs (optimal $E_{c.m.}$) for producing isotopes $^{295-302}$121 are ^{252}Es (^{46}Ti, 3n) ^{295}121, 4.123 fb (223.9 MeV), ^{248}Cf (^{50}V, 3n) ^{296}121, 0.566 fb (239.1 MeV), ^{254}Es (^{46}Ti, 3n) ^{297}121, 6.619 fb (219.9 MeV), ^{254}Es (^{47}Ti, 3n) ^{298}121, 1.331 fb (222.3 MeV), ^{257}Fm (^{45}Sc, 3n) ^{299}121, 8.778 fb (213.6 MeV), ^{254}Es (^{49}Ti, 3n) ^{300}121, 0.453 fb (228.5 MeV), ^{254}Cf (^{50}V, 3n) ^{301}121, 3.705 fb (229.0 MeV), and ^{254}Cf (^{51}V, 3n) ^{302}121, 0.524 fb (234.1 MeV).

As mentioned in the previous paragraph, the largest maximal ERCS corresponding to the synthesis of the SHE with Z = 121 is 8.778 fb in the reaction ^{45}Sc+^{257}Fm. In addition, the reactions ^{46}Ti+^{252}Es and ^{46}Ti+^{254}Es offer large maximal ERCSs of 4.123 and 6.619 fb, respectively. Considering its experimental feasibility, the ^{254}Es target is currently available among several Es targets in the laboratory [94], with a half-life of 275.70 d. The ^{252}Es target has a comparatively long half-life (1.29 y), making it a potential target for experimental purposes. Therefore, despite the slightly higher ERCS of the reaction ^{45}Sc+^{257}Fm, the reactions ^{46}Ti+^{252,254}Es are more feasible for experimental purposes.

In Fig. 2a–c, we present the calculated ERCSs of the reactions ^{45}Sc+^{257}Fm, ^{48}Ti+^{254}Es, and ^{51}V+^{251}Cf. These reactions yield the same compound nuclei of ^{302}121. Notably, our analysis revealed a consistently decreasing trend in the maximal ERCSs for synthesizing the same isotopes, ^{299}121 via the 3n-emission channel and ^{298}121 via the 4n-emission channel, as the charge number of the projectiles increased. This trend can be attributed to the reduced fusion probability resulting from the increased mass asymmetry. To further investigate the influence of mass asymmetry on the fusion-evaporation reaction, the fusion probabilities and driving potentials for the reactions ^{45}Sc+^{257}Fm, ^{48}Ti+^{254}Es, and ^{51}V+^{251}Cf are presented in Figs. 3 and 4.

Figure 3 reveals that the fusion probabilities exhibit an increasing trend with increasing E^*_{CN}. This occurred because of the heightened dissipated energy within the dinuclear system at higher E^*_{CN}, thus rendering the reaction system more likely to overcome the inner fusion barrier. Additionally, Fig. 3 shows that the reaction ^{45}Sc+^{257}Fm exhibits a much

Table 1 Favorable reaction systems for producing SHEs $Z = 121$

Isotope	Reaction	$T_{1/2}$(target)	$E_{c.m.}$ (MeV)	E^*_{CN} (MeV)	σ_{ER} (fb)
$^{295}121$	^{252}Es(^{46}Ti,3n)	1.29 yr	223.9	36.0	$4.123^{+5.52}_{-2.495}$
$^{296}121$	^{248}Cf(^{50}V,3n)	333.50 d	239.1	36.0	$0.566^{+0.758}_{-0.342}$
$^{297}121$	^{254}Es(^{46}Ti,3n)	275.70 d	219.9	35.0	$6.619^{+9.196}_{-4.073}$
	^{249}Cf(^{51}V,3n)	351.00 yr	240.3	35.0	$0.306^{+0.426}_{-0.188}$
$^{298}121$	^{254}Es(^{47}Ti,3n)	275.70 d	222.3	36.0	$1.331^{+1.827}_{-0.813}$
$^{299}121$	^{257}Fm(^{45}Sc,3n)	100.50 d	213.6	36.0	$8.778^{+11.923}_{-5.339}$
	^{254}Es(^{48}Ti,3n)	275.70 d	227.6	36.0	$1.677^{+2.293}_{-1.02}$
	^{252}Cf(^{50}V,3n)	2.64 yr	232.3	34.0	$1.368^{+1.936}_{-0.842}$
	^{251}Cf(^{51}V,3n)	898.00 yr	238.2	35.0	$0.540^{+0.748}_{-0.332}$
$^{300}121$	^{254}Es(^{49}Ti,3n)	275.70 d	228.5	36.0	$0.453^{+0.594}_{-0.272}$
$^{301}121$	^{254}Cf(^{50}V,3n)	60.50 d	229.0	33.0	$3.705^{+4.912}_{-2.249}$
	^{254}Es(^{50}Ti,3n)	275.70 d	232.5	35.0	$0.541^{+0.688}_{-0.321}$
$^{302}121$	^{254}Cf(^{51}V,3n)	60.50 d	234.1	34.0	$0.524^{+0.636}_{-0.306}$

The isotopes, reaction systems, and half-lives of corresponding targets [93] are presented in columns 1–3. The optimal incident energies $E_{c.m.}$ and E^*_{CN} are listed in columns 4–5, respectively. The maximal calculated ERCSs for certain neutron emission channels are shown in column 6

larger fusion probability than the other two reactions. Conversely, the reaction ^{51}V+^{251}Cf exhibits the lowest fusion probability. This significant difference can be attributed to the different B_{fus} values influenced by the change in mass asymmetry.

Figure 4 shows that as the mass asymmetry of the reaction system decreases, the entrance channel approaches the B.G. point, resulting in a corresponding decrease in B_{fus}. For the reaction ^{45}Sc+^{257}Fm, the B_{fus} is 13.1 MeV, which is lower than the reactions ^{48}Ti+^{254}Es (B_{fus}=17.1 MeV) and ^{51}V+^{251}Cf (B_{fus}=17.8 MeV). Consequently, the reaction ^{45}Sc+^{257}Fm is more likely to overcome the inner fusion barrier, resulting in an enhanced fusion probability, as shown in Fig. 3. Evidently, the heightened fusion probabilities, stemming from the reduced mass asymmetry, establish the superiority of Sc- and Ti-induced reactions for producing the SHE with $Z = 121$.

In Fig. 5, we present an analysis of the calculated maximal ERCSs, corresponding incident energies, and Q values for reactions involving $^{46-50}$Ti projectiles and ^{252,254}Es targets. Figure 5a reveals that the reactions employing the neutron-rich ^{254}Es target consistently yielded larger maximal ERCSs than those employing the ^{252}Es target. Moreover, the maximum ERCSs decreased as the neutron number of the projectile increased. Notably, odd–even effects also impact the maximal ERCSs, with even-A Ti projectiles resulting in relatively enhanced ERCSs. Figure 5b illustrates that the optimal incident energies for reactions with the ^{252}Es target are approximately 3–4 MeV higher than those with the ^{254}Es target. Additionally, the optimal incident energies exhibited a discernible increase, with evident odd–even effects as the neutron number of the projectiles increased.

For all reactions $^{46-50}$Ti+^{252}Es and $^{46-50}$Ti+^{254}Es, the corresponding E^*_{CN} falls within the range of 35–37 MeV. This range has a limited effect on the optimal incident energy. The increasing trend in the optimal incident energy can be attributed to the differences in the Q values. Figure 5c reveals that a high neutron excess of the target nuclei enhances the Q values of the reaction system, whereas a high neutron excess of the projectile nuclei exerts the opposite effect. The odd–even effects of the projectiles also have a significant influence on the Q values, with reactions utilizing even-A Ti projectiles displaying

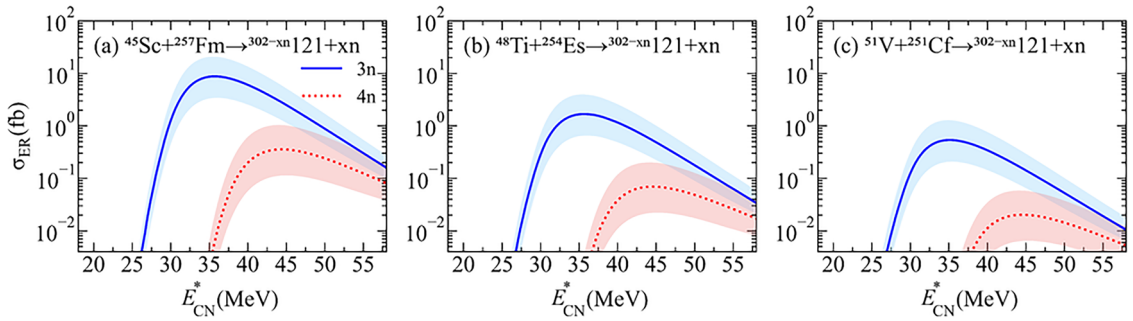

Fig. 2 (Color online) Predicted ERCSs of the reactions ^{45}Sc +^{257} Fm, ^{48}Ti +^{254} Es, and ^{51}V +^{251} Cf. The 3n- and 4n-emission channels are indicated by the blue solid and red dotted lines, respectively. The shades indicate the uncertainties of the calculated ERCSs

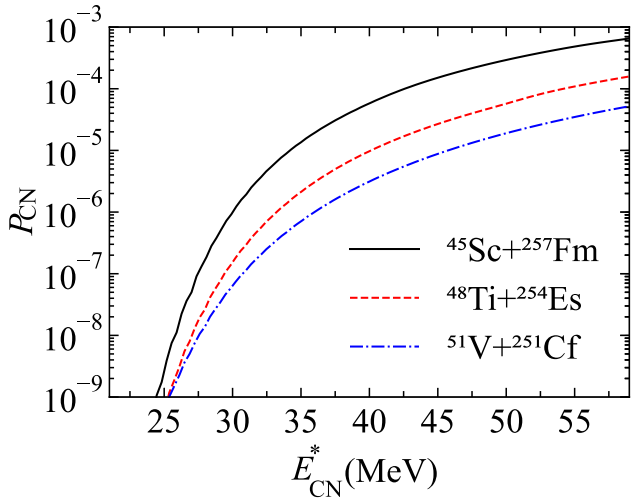

Fig. 3 (Color online) Calculated fusion probabilities of the reactions ^{45}Sc+^{257}Fm (black solid line), ^{48}Ti+^{254}Es (red dashed line), and ^{51}V+^{251}Cf (blue dash-dot line)

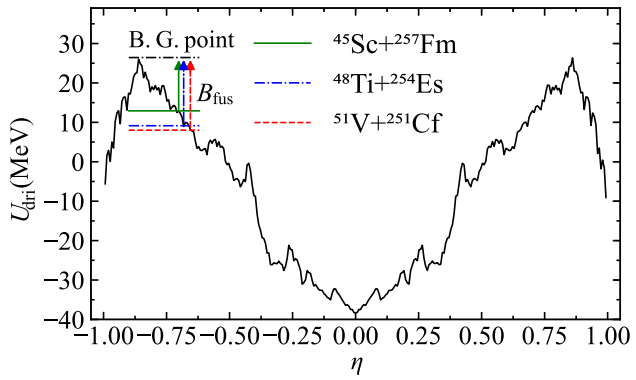

Fig. 4 (Color online) Driving potential for the reaction ^{45}Sc+^{257}Fm, ^{48}Ti+^{254}Es, and ^{51}V+^{251}Cf as a function of mass asymmetry. The arrows indicate the entrance channel

relatively suppressed Q values compared to those employing odd-A Ti projectiles.

A comprehensive investigation of the capture, fusion, and survival stages is essential for determining the isotopic dependence of the maximal ERCSs and the corresponding optimal incident energies. In Fig. 6a, we present the capture cross sections for the combinations involving $^{46-50}$Ti projectiles colliding with ^{252}Es and ^{254}Es targets at excitation energies of E^*_{CN} = 35 MeV and 50 MeV. Notably, the capture cross sections exhibit an increasing trend with increasing E^*_{CN}, as the ability to surpass the Coulomb barrier increases with higher E^*_{CN}. Furthermore, the capture cross sections of the reactions involving ^{252}Es targets are notably enhanced compared to those with ^{254}Es targets. Additionally, there is an upward trend in the capture cross sections with a higher neutron excess in the projectiles.

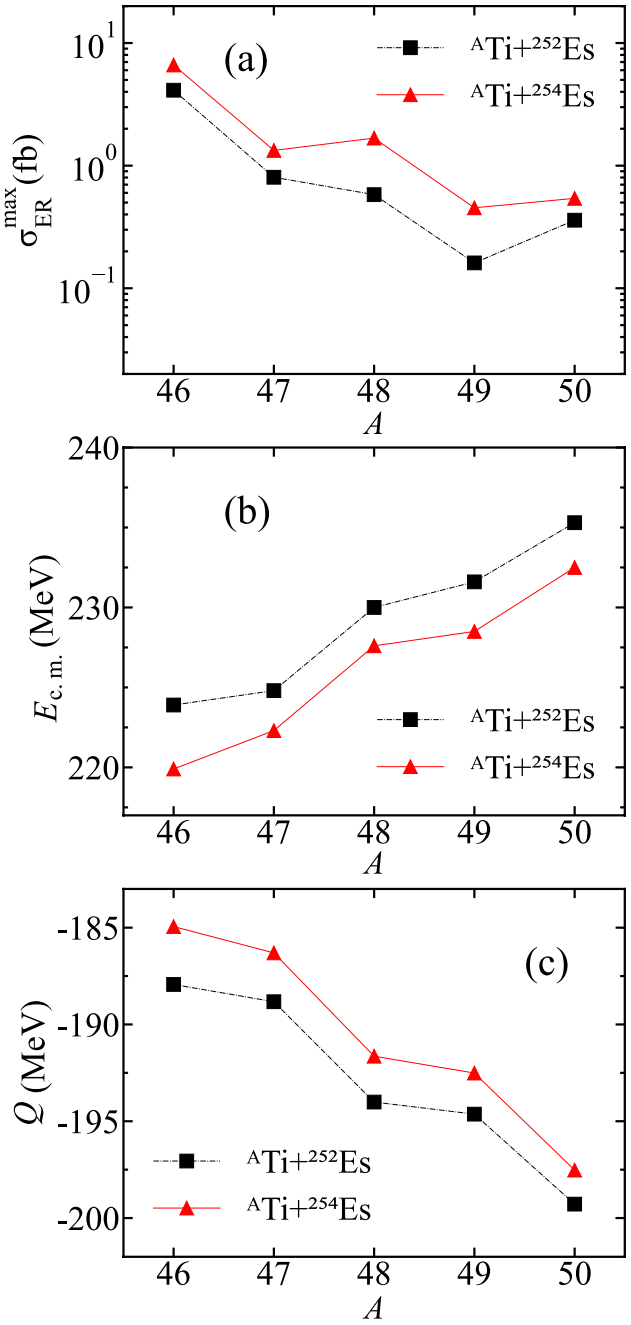

Fig. 5 (Color online) **a** Calculated maximal ERCSs, **b** corresponding optimal incident energies, and **c** the Q values of the reactions $^{46-50}$Ti+^{252}Es and $^{46-50}$Ti+^{254}Es

These trends can be attributed to a decrease in the Coulomb barrier.

In Fig. 6b, the excitation energies associated with the Coulomb barriers $V_b + Q$ of the corresponding reactions are plotted. The $V_b + Q$ values decreased with increasing neutron excess in the projectiles. Moreover, the reaction systems with the ^{252}Es target exhibited lower $V_b + Q$ values than those with ^{254}Es targets. Consequently, reactions

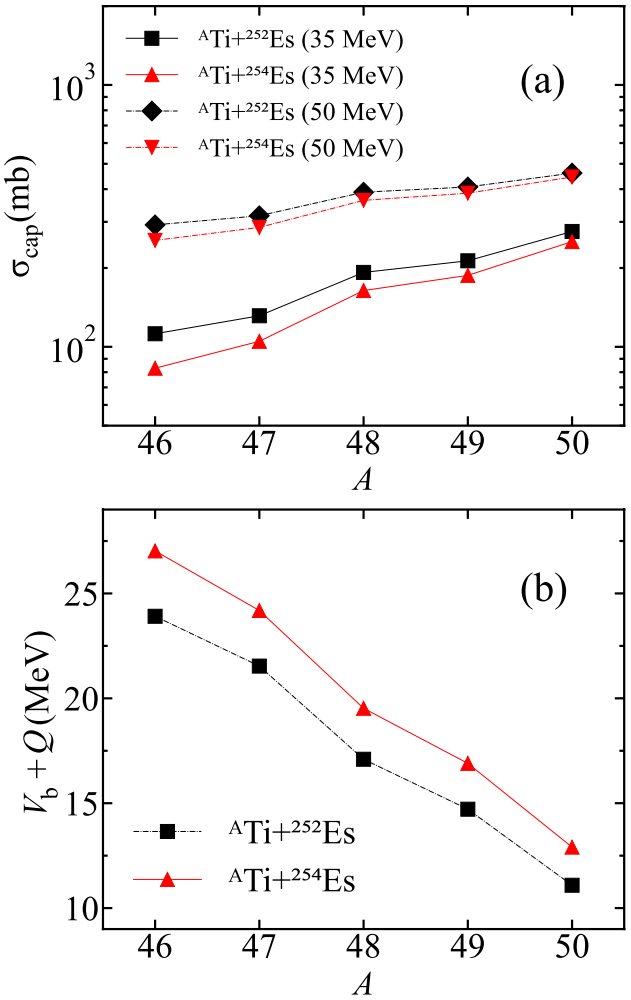

Fig. 6 (Color online) **a** Calculated capture cross sections of the reactions $^{46-50}$Ti+^{252}Es and $^{46-50}$Ti+^{254}Es with $E^*_{CN} = 35$ MeV and $E^*_{CN} = 50$ MeV. **b** Excitation energies of the corresponding Coulomb barriers $V_b + Q$ of the reactions $^{46-50}$Ti+^{252}Es and $^{46-50}$Ti+^{254}Es

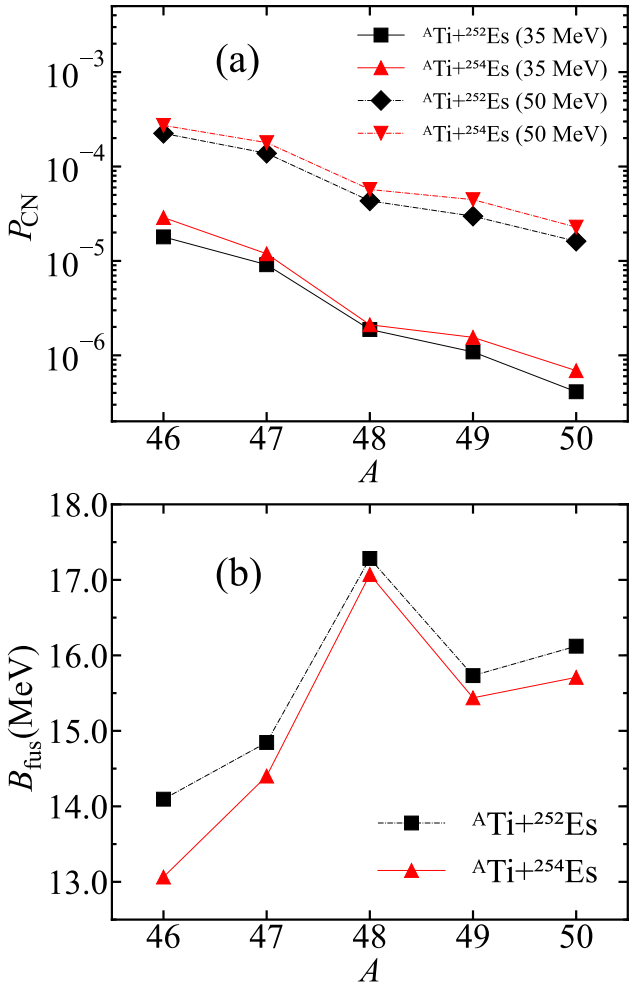

Fig. 7 (Color online) **a** Calculated fusion probabilities of the reactions $^{46-50}$Ti+^{252}Es and $^{46-50}$Ti+^{254}Es with $E^*_{CN} = 35$ MeV and $E^*_{CN} = 50$ MeV. **b** B_{fus} values of the reactions $^{46-50}$Ti+^{252}Es and $^{46-50}$Ti+^{254}Es

involving ^{252}Es as target nuclei coupled with neutron-rich Ti projectiles have an increased likelihood of overcoming the Coulomb barrier, thereby enhancing the corresponding capture cross sections.

The fusion process in Fig. 7a shows the fusion probabilities of reactions $^{46-50}$Ti+^{252}Es and $^{46-50}$Ti+^{254}Es at $E^*_{CN} = 35$ MeV and 50 MeV. As the probability of overcoming the inner fusion barrier increased, the fusion probabilities were amplified with a higher E^*_{CN}. These fusion probabilities exhibit a decreasing trend with increasing neutron excess in the projectile. Notably, the employment of the neutron-rich ^{254}Es target leads to a relative enhancement in the fusion probability, which can be attributed to the reduced inner fusion barrier. Figure 7b shows the inner fusion barriers for the corresponding reactions. Notably, the B_{fus} values increase with increasing neutron excess in the projectiles and are higher in reaction systems with lighter ^{252}Es targets. This can be attributed to the increased mass asymmetry of projectiles with a higher neutron excess and targets with a lower neutron excess, which subsequently enhances the B_{fus} values and hinders the fusion process.

In Fig. 8a, the survival probabilities of the compound nuclei in the 3n-emission channel for reactions $^{46-50}$Ti+^{252}Es and $^{46-50}$Ti+^{254}Es at $E^*_{CN} = 35$ MeV and 50 MeV are plotted. Notably, the survival probabilities exhibited a decreasing trend as E^*_{CN} increased. This is due to the damped shell effect at increased E^*_{CN}, which results in diminished compound nucleus stability. Additionally, the ^{254}Es-based reactions exhibited relatively high fusion probabilities with an evident odd–even staggering pattern. This can be ascribed to the influences of the B_n and B_f values of the corresponding

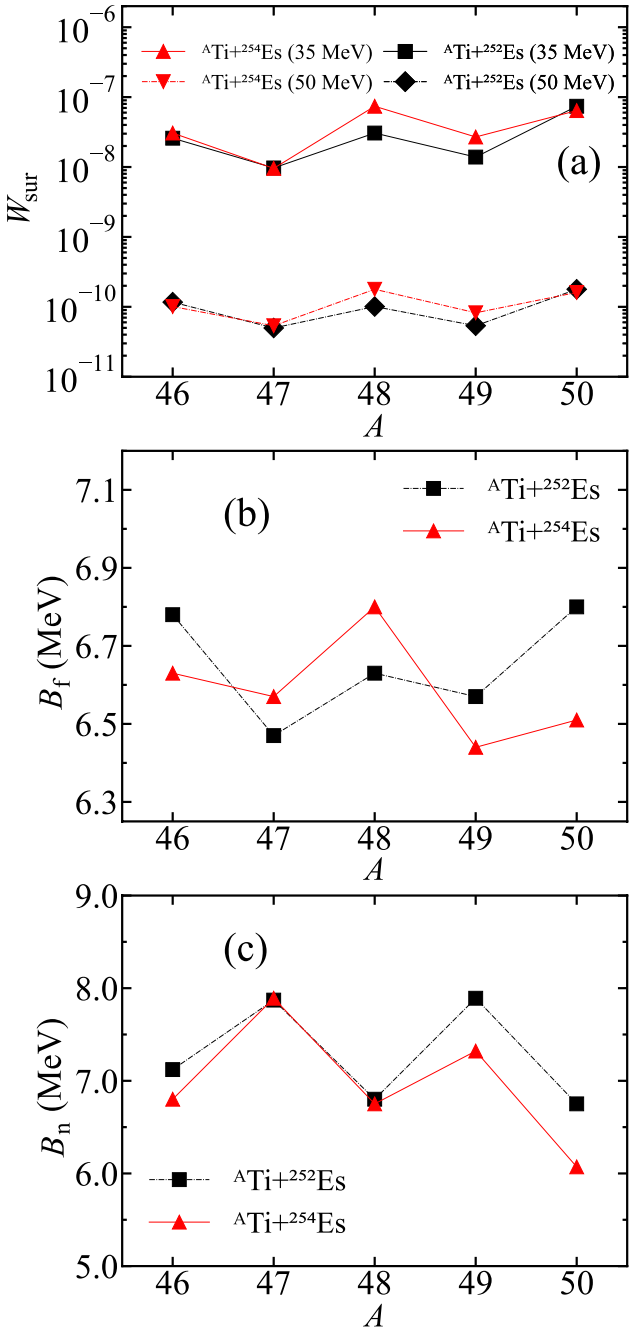

Fig. 8 (Color online) **a** Calculated survival probabilities of the compound nuclei in the 3n-emission channel for the reactions $^{46-50}$Ti+^{252}Es and $^{46-50}$Ti+^{254}Es with E^*_{CN} = 35 MeV and E^*_{CN} = 50 MeV. **b** B_f values and **c** B_n values of the corresponding compound nuclei

compound nuclei, as shown in Fig. 8b and c). The compound nuclei formed via the even-*A* projectiles are more likely to de-excite through neutron emission because of their relatively higher B_f values and lower B_n values. This behavior results in odd–even staggering in both the survival probabilities and maximal ERCSs of the Ti-induced reactions. Furthermore, the combined effect of the B_n and B_f values contributes to the generally higher survival probabilities in reactions with the ^{254}Es target compared with those with ^{252}Es targets. This dual enhancement in the fusion and survival stages highlights the advantage of employing a ^{254}Es target for the synthesis of isotopes with $Z = 121$.

4 Summary

The calculated ERCSs using the DNS model were assessed using the experimental results of the reactions ^{48}Ca + ^{245}Cm, ^{48}Ca + ^{248}Cm, ^{48}Ca + ^{249}Bk, and ^{48}Ca + ^{249}Cf. Our analysis indicates consistency between the theoretical predictions and the experimental results. Based on the DNS model, we investigated the synthesis of the SHE $Z = 121$ using stable projectiles with $Z = 21 - 30$ and actinide targets with half-lives longer than 50 d, revealing that this element is expected to be produced via reactions ^{45}Sc+^{257}Fm, ^{46}Ti + ^{254}Es, and ^{46}Ti + ^{252}Es. Considering the experimental feasibility, the reactions ^{46}Ti + ^{254}Es and ^{46}Ti + ^{252}Es are more favorable with maximal ERCSs and optimal incident energies of 6.619 fb at 219.9 MeV and 4.123 fb at 223.9 MeV.

We investigated the mass asymmetry effect, revealing enhanced fusion probabilities for Sc- and Ti-induced reactions. Additionally, the influences of the *Q* values, Coulomb barriers, inner fusion barriers, fission barriers, and neutron separation energies on the isotopic dependence of the reactions with Ti projectiles and Es targets were analyzed in detail. Our results indicate that employing a ^{254}Es target and even-*A* Ti projectiles with a smaller neutron excess is favorable for synthesizing the element $Z = 121$.

Author Contributions All authors contributed to the study conception and design. Material preparation, data collection and analysis were performed by Ming-Hao Zhang, Yu-Hai Zhang, Ying Zou, Xiu-Xiu Yang, Gen Zhang, and Feng-Shou Zhang. The first draft of the manuscript was written by Ming-Hao Zhang and all authors commented on previous versions of the manuscript. All authors read and approved the final manuscript.

Data Availability Statement The data that support the findings of this study are openly available in Science Data Bank at https://cstr.cn/31253.11.sciencedb.j00186.00527 and https://doi.org/10.57760/sciencedb.j00186.00527.

Declarations

Conflict of interest Feng-Shou Zhang is an editorial board member for Nuclear Science and Techniques and was not involved in the editorial review, or the decision to publish this article. All authors declare that there are no Conflict of interest.

References

1. A. Sobiczewski, F.A. Gareev, B.N. Kalinkin, Closed shells for $Z > 82$ and $N > 126$ in a diffuse potential well. Phys. Lett. **22**, 500–502 (1966). https://doi.org/10.1016/0031-9163(66)91243-1
2. P. Möller, J.R. Nix, Stability of heavy and superheavy elements. J. Phys. G Nucl. Part. Phys. **20**, 1681–1747 (1994). https://doi.org/10.1088/0954-3899/20/11/003
3. S. Ćwiok, P.-H. Heenen, W. Nazarewicz, Shape coexistence and triaxiality in the superheavy nuclei. Nature **433**, 705–709 (2005). https://doi.org/10.1038/nature03336
4. S. Hofmann, G. Münzenberg, The discovery of the heaviest elements. Rev. Mod. Phys. **72**, 733–767 (2000). https://doi.org/10.1103/RevModPhys.72.733
5. K. Morita, K. Morimoto, D. Kaji et al., Experiment on the synthesis of element 113 in the reaction ^{209}Bi (^{70}Zn, n) ^{278}113. J. Phys. Soc. Jpn. **73**, 2593–2596 (2004). https://doi.org/10.1143/jpsj.73.2593
6. Y.T. Oganessian, V.K. Utyonkov, Y.V. Lobanov et al., Attempt to produce element 120 in the ^{244}Pu+ ^{58}Fe reaction. Phys. Rev. C **79**, 024603 (2009). https://doi.org/10.1103/PhysRevC.79.024603
7. Y.T. Oganessian, V.K. Utyonkov, Super-heavy element research. Rep. Prog. Phys. **78**, 036301 (2015). https://doi.org/10.1088/0034-4885/78/3/036301
8. Y.T. Oganessian, A.V. Yeremin, A.G. Popeko et al., Synthesis of nuclei of the superheavy element 114 in reactions induced by ^{48}Ca. Nature **400**, 242–245 (1999). https://doi.org/10.1038/22281
9. Y.T. Oganessian, F.S. Abdullin, S.N. Dmitriev et al., Investigation of the ^{243}Am+ ^{48}Ca reaction products previously observed in the experiments on elements 113, 115, and 117. Phys. Rev. C **87**, 014302 (2013). https://doi.org/10.1103/PhysRevC.87.014302
10. Y.T. Oganessian, V.K. Utyonkov, Y.V. Lobanov et al., Observation of the decay of ^{292}116. Phys. Rev. C **63**, 011301(R) (2000). https://doi.org/10.1103/PhysRevC.63.011301
11. Y.T. Oganessian, F.S. Abdullin, P.D. Bailey et al., Synthesis of a new element with atomic number $Z = 117$. Phys. Rev. Lett. **104**, 142502 (2010). https://doi.org/10.1103/PhysRevLett.104.142502
12. Y.T. Oganessian, V.K. Utyonkov, Y.V. Lobanov et al., Synthesis of the isotopes of elements 118 and 116 in the ^{249}Cf and ^{245}Cm+ ^{48}Ca fusion reactions. Phys. Rev. C **74**, 044602 (2006). https://doi.org/10.1103/PhysRevC.74.044602
13. S. Hofmann, Synthesis of superheavy elements by cold fusion. Radiochim. Acta **99**, 405–428 (2011). https://doi.org/10.1524/ract.2011.1854
14. A.V. Yeremin, Regularities of formation and survival probability of compound nuclei in the region of $Z \geq 82$: study of complete-fusion reactions with heavy ions using the kinematic separator VASSILISSA. Phys. Part. Nucl. **38**, 492–524 (2007). https://doi.org/10.1134/S1063779607040041
15. Z.Y. Zhang, Z.G. Gan, L. Ma et al., Observation of the superheavy nuclide ^{271}Ds. Chin. Phys. Lett. **29**, 012502 (2012). https://doi.org/10.1088/0256-307X/29/1/012502
16. Y.T. Oganessian, V.K. Utyonkov, N.D. Kovrizhnykh et al., New isotope ^{286}Mc produced in the ^{243}Am+^{48}Ca reaction. Phys. Rev. C **106**, 064306 (2022). https://doi.org/10.1103/PhysRevC.106.064306
17. S. Hofmann, S. Heinz, R. Mann et al., Review of even element super-heavy nuclei and search for element 120. Eur. Phys. J. A **52**, 180–213 (2016). https://doi.org/10.1140/epja/i2016-16180-4
18. F. Heßberger, D. Ackermann, Some critical remarks on a sequence of events interpreted to possibly originate from a decay chain of an element 120 isotope. Eur. Phys. J. A **53**, 123–131 (2017). https://doi.org/10.1140/epja/i2017-12307-5
19. J. Khuyagbaatar, A. Yakushev, C.E. Düllmann et al., Search for elements 119 and 120. Phys. Rev. C **102**, 064602 (2020). https://doi.org/10.1103/PhysRevC.102.064602
20. M. Tanaka, P. Brionnet, M. Du et al., Probing optimal reaction energy for synthesis of element 119 from ^{51}V+^{248}Cm reaction with quasielastic barrier distribution measurement. J. Phys. Soc. Jpn. **91**, 084201 (2022). https://doi.org/10.7566/JPSJ.91.084201
21. Y.H. Zhang, G. Zhang, J.J. Li et al., Production cross sections of $^{243-248}$No isotopes in fusion reactions. Phys. Rev. C **106**, 014625 (2022). https://doi.org/10.1103/PhysRevC.106.014625
22. K. Sekizawa, K. Hagino, Time-dependent Hartree–Fock plus Langevin approach for hot fusion reactions to synthesize the Z=120 superheavy element. Phys. Rev. C **99**, 051602(R) (2019). https://doi.org/10.1103/PhysRevC.99.051602
23. L. Li, L. Guo, K. Godbey et al., Impact of tensor force on quantum shell effects in quasifission reactions. Phys. Lett. B **833**, 137349 (2022). https://doi.org/10.1016/j.physletb.2022.137349
24. X.X. Sun, L. Guo, Microscopic study of fusion reactions with a weakly bound nucleus: effects of deformed halo. Phys. Rev. C **107**, L011601 (2023). https://doi.org/10.1103/PhysRevC.107.L011601
25. X.X. Sun, L. Guo, Microscopic study of the hot-fusion reaction ^{48}Ca +^{238} U with the constraints from time-dependent Hartree–Fock theory. Phys. Rev. C **107**, 064609 (2023). https://doi.org/10.1103/PhysRevC.107.064609
26. T. Cap, M. Kowal, K. Siwek-Wilczynska, The fusion-by-diffusion model as a tool to calculate cross sections for the production of superheavy nuclei. Eur. Phys. J. A **58**, 231–248 (2022). https://doi.org/10.1140/epja/s10050-022-00891-8
27. S. Chopra, M.K. Sharma, P.O. Hess et al., Possibility to form Z=120 via the ^{64}Ni+^{238}U reaction using the dynamical cluster-decay model. Phys. Rev. C **105**, 014610 (2022). https://doi.org/10.1103/PhysRevC.105.014610
28. D. Boilley, Y. Abe, B. Cauchois et al., Elimination of fast variables and initial slip: a new mechanism for fusion hindrance in heavy-ion collisions. J. Phys. G Nucl. Part. Phys. **46**, 115102 (2019). https://doi.org/10.1088/1361-6471/ab11ef
29. L. Liu, C.W. Shen, Q.F. Li et al., Residue cross sections of ^{50}Ti-induced fusion reactions based on the two-step model. Eur. Phys. J. A **52**, 35–39 (2016). https://doi.org/10.1140/epja/i2016-16035-0
30. G.G. Adamian, N.V. Antonenko, W. Scheid et al., Fusion cross sections for superheavy nuclei in the dinuclear system concept. Nucl. Phys. A **633**, 409–420 (1998). https://doi.org/10.1016/S0375-9474(98)00124-9
31. G. Zhang, C.A.T. Sokhna, Z. Liu et al., Production of neutron-rich isotopes ^{264,266,268,269}Rf by multinucleon transfer reactions based on ^{238}U beam. Phys. Rev. C **100**, 024613 (2019). https://doi.org/10.1103/PhysRevC.100.024613
32. L. Zhu, J. Su, F.S. Zhang, Influence of the neutron numbers of projectile and target on the evaporation residue cross sections in hot fusion reactions. Phys. Rev. C **93**, 064610 (2016). https://doi.org/10.1103/PhysRevC.93.064610
33. F. Li, L. Zhu, Z.H. Wu et al., Predictions for the synthesis of superheavy elements $Z = 119$ and 120. Phys. Rev. C **98**, 014618 (2018). https://doi.org/10.1103/PhysRevC.98.014618
34. P.W. Wen, A.K. Nasirov, C.J. Lin et al., Multinucleon transfer reaction from view point of dynamical dinuclear system method. J. Phys. G Nucl. Part. Phys. **47**, 075106 (2020). https://doi.org/10.1088/1361-6471/ab8dcc
35. N. Wang, E.G. Zhao, W. Scheid et al., Theoretical study of the synthesis of superheavy nuclei with Z=119 and 120 in heavy-ion reactions with trans-uranium targets. Phys. Rev. C **85**, 041601(R) (2012). https://doi.org/10.1103/PhysRevC.85.041601
36. X.J. Bao, S.Q. Guo, H.F. Zhang et al., Influence of entrance channel on production cross sections of superheavy nuclei. Phys.

Rev. C **96**, 024610 (2017). https://doi.org/10.1103/PhysRevC.85.041601
37. X.B. Yu, L. Zhu, Z.H. Wu et al., Predictions for production of superheavy nuclei with z = 105–112 in hot fusion reactions. Nucl. Sci. Tech. **29**, 154 (2018). https://doi.org/10.1007/s41365-018-0501-2
38. P.H. Chen, H. Wu, Z.X. Yang et al., Prediction of synthesis cross sections of new moscovium isotopes in fusion-evaporation reactions. Nucl. Sci. Tech. **34**, 7 (2023). https://doi.org/10.1007/s41365-022-01157-0
39. C. Li, P.W. Wen, J.J. Li et al., Production of heavy neutron-rich nuclei with radioactive beams in multinucleon transfer reactions. Nucl. Sci. Tech. **28**, 110 (2017). https://doi.org/10.1007/s41365-017-0266-z
40. M.T. Jin, S.Y. Xu, G.M. Yang et al., Yield of long-lived fission product transmutation using proton-, deuteron-, and alpha particle-induced spallation. Nucl. Sci. Tech. **32**, 96 (2021). https://doi.org/10.1007/s41365-021-00933-8
41. M.H. Zhang, Y.H. Zhang, Y. Zou et al., Predictions of synthesizing elements with Z = 119 and 120 in fusion reactions. Phys. Rev. C **109**, 014622 (2024). https://doi.org/10.1103/PhysRevC.109.014622
42. P.H. Chen, C. Geng, Z.X. Yang et al., Production of neutron-rich actinide isotopes in isobaric collisions via multinucleon transfer reactions. Nucl. Sci. Tech. **34**, 160 (2023). https://doi.org/10.1007/s41365-023-01314-z
43. S.Y. Xu, Z.Q. Feng, Cluster emission in massive transfer reactions based on dinuclear system model. Nucl. Tech **46**, 030501 (2023). https://doi.org/10.11889/j.0253-3219.2023.hjs.46.030501. (**in Chinese**)
44. M.H. Zhang, Y.H. Zhang, J.J. Li et al., Progress in transport models of heavy-ion collisions for the synthesis of superheavy nuclei. Nucl. Tech **46**, 137 (2023). https://doi.org/10.11889/j.0253-3219.2023.hjs.46.080014. (**in Chinese**)
45. L. Zhu, W.J. Xie, F.S. Zhang, Production cross sections of superheavy elements Z = 119 and 120 in hot fusion reactions. Phys. Rev. C **89**, 024615 (2014). https://doi.org/10.1103/PhysRevC.89.024615
46. X.J. Lv, Z.Y. Yue, W.J. Zhao et al., Theoretical study of evaporation-residue cross sections of superheavy nuclei. Phys. Rev. C **103**, 064616 (2021). https://doi.org/10.1103/PhysRevC.103.064616
47. N. Wang, J.L. Tian, W. Scheid, Systematics of fusion probability in "hot'' fusion reactions. Phys. Rev. C **84**, 061601(R) (2011). https://doi.org/10.1103/PhysRevC.84.061601
48. N. Wang, X. Wu, Z. Li et al., Applications of skyrme energy-density functional to fusion reactions for synthesis of superheavy nuclei. Phys. Rev. C **74**, 044604 (2006). https://doi.org/10.1103/PhysRevC.74.044604
49. X.J. Bao, Possibilities for synthesis of new neutron-deficient isotopes of superheavy nuclei*. Chin. Phys. C **43**, 054105 (2019). https://doi.org/10.1088/1674-1137/43/5/054105
50. J.X. Li, H.F. Zhang, Predictions for the synthesis of the Z=120 superheavy element. Phys. Rev. C **106**, 034613 (2022). https://doi.org/10.1103/PhysRevC.106.034613
51. X.Q. Deng, S.G. Zhou, Examination of promising reactions with ^{241}Am and ^{244}Cm targets for the synthesis of new superheavy elements within the dinuclear system model with a dynamical potential energy surface. Phys. Rev. C **107**, 014616 (2023). https://doi.org/10.1103/PhysRevC.107.014616
52. B.M. Kayumov, O.K. Ganiev, A.K. Nasirov et al., Analysis of the fusion mechanism in the synthesis of superheavy element 119 via the ^{54}Cr+^{243}Am reaction. Phys. Rev. C **105**, 014618 (2022). https://doi.org/10.1103/PhysRevC.105.014618
53. J. Hong, G.G. Adamian, N.V. Antonenko et al., Hot and cold fusion reactions leading to the same superheavy evaporation residue. Eur. Phys. J. A **58**, 180–183 (2022). https://doi.org/10.1140/epja/s10050-022-00826-3
54. K.X. Cheng, J. Pu, Y.T. Wang et al., Non-frozen process of heavy-ion fusion reactions at deep sub-barrier energies. Nucl. Sci. Tech. **33**, 132 (2022). https://doi.org/10.1007/s41365-022-01114-x
55. B. Li, N. Tang, Y.H. Zhang et al., Production of p-rich nuclei with z= 20–25 based on radioactive ion beams. Nucl. Sci. Tech. **33**, 55 (2022). https://doi.org/10.1007/s41365-022-01048-4
56. T.P. Luo, P.W. Wen, C.J. Lin et al., Bayesian analysis on non-resonant behavior of ^{12}C + ^{12}C fusion reaction at sub-barrier energies. Chin. Phys. C **46**, 064105 (2022). https://doi.org/10.1088/1674-1137/ac5587
57. S.H. Zhu, X.J. Bao, Possibility to synthesize Z = 120 superheavy nuclei with Z > 20 projectiles. Phys. Rev. C **108**, 014604 (2023). https://doi.org/10.1103/PhysRevC.108.014604
58. B.S. Cai, C.X. Yuan, Random forest-based prediction of decay modes and half-lives of superheavy nuclei. Nucl. Sci. Tech. **34**, 204 (2023). https://doi.org/10.1007/s41365-023-01354-5
59. Z. Wang, Z.Z. Ren, Predictions of the decay properties of the superheavy nuclei ^{293,294}119 and ^{294,295}120. Nucl. Tech **46**, 114 (2023). https://doi.org/10.11889/j.0253-3219.2023.hjs.46.080011. (**in Chinese**)
60. V.I. Zagrebaev, Synthesis of superheavy nuclei: nucleon collectivization as a mechanism for compound nucleus formation. Phys. Rev. C **64**, 034606 (2001). https://doi.org/10.1103/PhysRevC.64.034606
61. A.S. Zubov, G.G. Adamian, N.V. Antonenko et al., Survival probability of superheavy nuclei. Phys. Rev. C **65**, 024308 (2002). https://doi.org/10.1103/PhysRevC.65.024308
62. Z.Q. Feng, G.M. Jin, F. Fu et al., Production cross sections of superheavy nuclei based on dinuclear system model. Nucl. Phys. A **771**, 50–67 (2006). https://doi.org/10.1016/j.nuclphysa.2006.03.002
63. W.D. Myers, W.J. Swiatecki, Nuclear masses and deformations. Nucl. Phys. **81**, 1–60 (1966). https://doi.org/10.1016/0029-5582(66)90639-0
64. C.Y. Wong, Interaction barrier in charged-particle nuclear reactions. Phys. Rev. Lett. **31**, 766–769 (1973). https://doi.org/10.1103/PhysRevLett.31.766
65. Z. Ahmed, Tunnelling through the morse barrier. Phys. Lett. A **157**, 1–5 (1991). https://doi.org/10.1016/0375-9601(91)90399-S
66. V.Y. Denisov, Expression for the heavy-ion fusion cross section. Phys. Rev. C **107**, 054618 (2023). https://doi.org/10.1103/PhysRevC.107.054618
67. S. Rana, R. Kumar, S. Patra et al., Fusion dynamics of astrophysical reactions using different transmission coefficients. Eur. Phys. J. A **58**, 241 (2022). https://doi.org/10.1140/epja/s10050-022-00893-6
68. B. Wang, K. Wen, W.J. Zhao et al., Systematics of capture and fusion dynamics in heavy-ion collisions. At. Data Nucl. Data Tables **114**, 281–370 (2017). https://doi.org/10.1016/j.adt.2016.06.003
69. P. Möller, A. Sierk, T. Ichikawa et al., Nuclear ground-state masses and deformations: FRDM(2012). At. Data Nucl. Data Tables **109–110**, 1–204 (2016). https://doi.org/10.1016/j.adt.2015.10.002
70. N. Wang, L. Dou, E.G. Zhao et al., Nuclear hexadecapole deformation effects on the production of super-heavy elements. Chin. Phys. Lett. **27**, 062502 (2010). https://doi.org/10.1088/0256-307X/27/6/062502
71. J.Q. Li, G. Wolschin, Distribution of the dissipated angular momentum in heavy-ion collisions. Phys. Rev. C **27**, 590–601 (1983). https://doi.org/10.1103/PhysRevC.27.590
72. S. Ayik, B. Schürmann, W. Nörenberg, Microscopic transport theory of heavy-ion collisions. Z. Phys. A **277**, 299–310 (1976). https://doi.org/10.1007/BF01415605

73. G.G. Adamian, N.V. Antonenko, W. Scheid, Characteristics of quasifission products within the dinuclear system model. Phys. Rev. C **68**, 034601 (2003). https://doi.org/10.1103/PhysRevC.68.034601
74. X.J. Bao, Y. Gao, J.Q. Li et al., Influence of the nuclear dynamical deformation on production cross sections of superheavy nuclei. Phys. Rev. C **91**, 011603 (2015). https://doi.org/10.1103/PhysRevC.91.011603
75. J.D. Jackson, A schematic model for (p, xn) cross sections in heavy elements. Can. J. Phys. **34**, 767–779 (1956). https://doi.org/10.1139/p56-087
76. V. Weisskopf, Statistics and nuclear reactions. Phys. Rev. **52**, 295–303 (1937). https://doi.org/10.1103/PhysRev.52.295
77. A.V. Ignatyuk, K.K. Istekov, G.N. Smirenkin, Role of the collective effects in a systematics of nuclear level density. Sov. J. Nucl. Phys. **29**, 875 (1979)
78. M. Blann, Decay of deformed and superdeformed nuclei formed in heavy ion reactions. Phys. Rev. C **21**, 1770–1782 (1980). https://doi.org/10.1103/PhysRevC.21.1770
79. N. Bohr, J.A. Wheeler, The mechanism of nuclear fission. Phys. Rev. **56**, 426–450 (1939). https://doi.org/10.1103/PhysRev.56.426
80. G.G. Adamian, N.V. Antonenko, S.P. Ivanova et al., Analysis of survival probability of superheavy nuclei. Phys. Rev. C **62**, 064303 (2000). https://doi.org/10.1103/PhysRevC.62.064303
81. A.S. Zubov, G.G. Adamian, N.V. Antonenko et al., Survival probabilities of superheavy nuclei based on recent predictions of nuclear properties. Eur. Phys. J. A **23**, 249 (2005). https://doi.org/10.1140/epja/i2004-10089-5
82. L. Zhu, Selection of projectiles for producing trans-uranium nuclei in transfer reactions within the improved dinuclear system model. J. Phys. G Nucl. Part. Phys. **47**, 065107 (2020). https://doi.org/10.1088/1361-6471/ab871f
83. V.Y. Denisov, I.Y. Sedykh, Calculation of the fission width of an excited nucleus with the fission barrier dependent on excitation energy. Phys. Rev. C **98**, 024601 (2018). https://doi.org/10.1103/PhysRevC.98.024601
84. W.F. Li, Z.Z. Wang, H.S. Xu et al., Odd-even effects of the survival probability for superheavy compound nuclei. Chin. Phys. Lett. **21**, 636 (2004). https://doi.org/10.1088/0256-307X/21/4/013
85. C.J. Xia, B.X. Sun, E.G. Zhao et al., Systematic study of survival probability of excited superheavy nuclei. Sci. China Phys. Mech. Astron. **54**, 109–113 (2011). https://doi.org/10.1007/s11433-011-4438-2
86. Y.T. Oganessian, V.K. Utyonkov, Y.V. Lobanov et al., Measurements of cross sections for the fusion-evaporation reactions ^{244}Pu (^{48}Ca, xn) $^{292-x}$114 and ^{245}Cm (^{48}Ca, xn) $^{293-x}$116. Phys. Rev. C **69**, 054607 (2004). https://doi.org/10.1103/PhysRevC.69.054607
87. Y.T. Oganessian, V.K. Utyonkov, Y.V. Lobanov et al., Measurements of cross sections and decay properties of the isotopes of elements 112, 114, and 116 produced in the fusion reactions ^{233,238}U, ^{242}Pu, and ^{248}Cm+^{48}Ca. Phys. Rev. C **70**, 064609 (2004). https://doi.org/10.1103/PhysRevC.70.064609
88. Y.T. Oganessian, F.S. Abdullin, C. Alexander et al., Studies of the ^{249}Bk+ ^{48}Ca reaction including decay properties and excitation function for isotopes of element 117 and discovery of the new isotope ^{277}Mt. Phys. Rev. C **87**, 054621 (2013). https://doi.org/10.1103/PhysRevC.87.054621
89. Y.T. Oganessian, F.S. Abdullin, C. Alexander et al., Production and decay of the heaviest nuclei ^{293,294}117 and ^{294}118. Phys. Rev. Lett. **109**, 162501 (2012). https://doi.org/10.1103/PhysRevLett.109.162501
90. A.A. Voinov, Y.T. Oganessian, F.S. Abdullin et al., Study of the $^{249-251}$Cf+ ^{48}Ca reactions: recent results and outlook. J. Phys Conf. Ser. **966**, 012057 (2018). https://doi.org/10.1088/1742-6596/966/1/012057
91. H. Lü, D. Boilley, Y. Abe et al., Synthesis of superheavy elements: uncertainty analysis to improve the predictive power of reaction models. Phys. Rev. C **94**, 034616 (2016). https://doi.org/10.1103/PhysRevC.94.034616
92. J.A. Sheikh, W. Nazarewicz, J.C. Pei, Systematic study of fission barriers of excited superheavy nuclei. Phys. Rev. C **80**, 011302(R) (2009). https://doi.org/10.1103/PhysRevC.80.011302
93. F.G. Kondev, M. Wang, W.J. Huang et al., The NUBASE2020 evaluation of nuclear physics properties. Chin. Phys. C **45**, 030001 (2021). https://doi.org/10.1088/1674-1137/abddae
94. R.W. Lougheed, J.H. Landrum, E.K. Hulet et al., Search for superheavy elements using the ^{48}Ca+^{254}Es^{g} reaction. Phys. Rev. C **32**, 1760–1763 (1985). https://doi.org/10.1103/PhysRevC.32.1760